Journal of Thermal Analysis, Vol. 51 (1998) 9-27

THERMAL ANALYSIS OF PHASE TRANSITIONS IN MICROEMULSIONS

D. Vollmer[1], *J. Vollmer*[2], *R. Strey*[3], *H.-G. Schmidt*[4] *and G. Wolf*[4]

[1]Institute for Physical Chemistry, University of Mainz, 55099 Mainz
[2]Department of Physics, University of Essen, 45117 Essen
[3]Institute for Physical Chemistry, University of Cologne, 50930 Köln
[4]Institute for Physical Chemistry, Technical University of Freiberg, 09596 Freiberg, Germany

Abstract

Differential scanning microcalorimetric measurements on phase transitions in water-oil-surfactant mixtures are presented, demonstrating that this method is highly sensitive towards small heat changes connected with structural transitions in the samples. The values for the latent heat of phase transitions are determined and the results are compared with predictions from mean field theory, emphasizing the role calorimetric experiments can play to identify the most important contributions to the free energy describing the mixtures. Doing this, the present status of the understanding of temperature dependent phase transitions in microemulsions is reviewed.

Keywords: bending free energy, calorimetry, latent heat, microemulsions, phase transitions

Introduction

Water-oil-surfactant mixtures form thermodynamically stable mixtures where a monolayer of surfactant is located at the interface between water and oil domains, reducing the interfacial tension between water and oil by several orders of magnitude [1–7]. A variety of different phases have been observed, depending on composition, temperature and electrolyte concentration in the water [2, 8–13]. Typical length scales of the underlying microstructures vary from a few Angstroms up to tens of nanometers [14, 15]. A detailed knowledge of the microstructures and the conditions under which they are formed is important for a technical use of these mixtures [16]. The aim of the present article is to show that most of these phase transitions are calorimetrically accessible and that their heat changes give clues for a theoretical description of the systems. Doing this we concentrate on a description of the transitions in ternary mixtures of water, alkane and the non-ionic surfactant $C_{12}E_5$ (*n*-dodecyl pentaethylene glycol ether).

A schematic phase diagram using a symmetric nonionic surfactant and equal volume fraction of water and oil is shown in Fig. 1 as function of temperature and

0368–4466/98/ $ 5.00

Akadémiai Kiadó, Budapest
Kluwer Academic Publishers, Dordrecht

surfactant concentration. The phase diagram is mirror symmetric with respect to $T=\underline{T}$. For $T\leq\overline{T}$ the monolayer is curved on the average towards oil, whereas for $T\geq\overline{T}$ it is curved towards water. For low surfactant concentrations $\phi_s\leq\underline{\phi}$ a three phase region (3Φ) is formed. Here, an oil and water continuous microemulsion is in equilibrium with a water- and an oil-rich phase. For temperatures below the lower phase boundary ($\underline{2\Phi}$) the water rich phase disappears and an oil rich phase is in equilibrium with typically an oil-droplet or an oil-cylindrical microemulsion. Analogously, for temperatures above the upper phase boundary ($\overline{2\Phi}$) typically a water-droplet or water-cylindrical microemulsion is in equilibrium with a water rich phase. Under increasing surfactant concentration the mixture becomes single phase. Close to $T=\overline{T}$ the three phase region is followed up by a single phase bicontinuous microemulsion. For still higher surfactant concentration a lamellar phase L_α is found. The lamellar phase is bounded by two microemulsion phases, enclosing oil (lower 1Φ channel, L_1) or water (upper 1Φ channel, L_2), which are separated from the lamellar phase by a two-phase region. Within a single phase microemulsion (L_1 and L_2-regions) the microstructure may conform to a droplet, to a cylindrical or to a bicontinuous one [17–22]. The respective morphology changes under variation of temperature or composition.

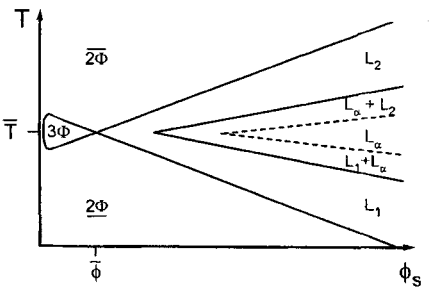

Fig. 1 Schematic phase diagram of a liquid mixture of water, oil and a symmetric nonionic surfactant. The phase behavior for equal volume fractions of water and oil ($\phi_w=\phi_o$) is shown as a function of temperature T and surfactant concentration ϕ_s

In contrast to the comparatively good experimental characterization of the phase diagrams, there is little knowledge about thermal properties of the mixtures [23–25], and their theoretical description is controversial [26–31]. Calorimetric investigations of temperature induced phase transitions provide supplementary experimental data which help to fill in these gaps. In detailed studies of the parameter dependence of the latent heat of selected transitions it has been demonstrated that these data can help to identify the role of different contributions to model free energies describing the phase behavior [25, 32].

In the present paper we take a slightly different point of view. In order to survey the status of calorimetric studies on the systems, we restrict ourselves to only two compositions, but discuss all transitions in these mixtures. In the section

'Experimantal results' we first give some basic information about the experiment, and subsequently discuss the heat curves of microcalorimetric measurements. The latent heat of transitions obtained from these experiments, is then compared to predictions of a mean field theory which is discussed in the section 'Theory'. In the concluding section the main results are summarized.

Experimental results

System preparation and experimental setup

The investigated mixtures are prepared from deionized, bidistilled water, highest grade commercially available octane (Fluka, Switzerland) and the nonionic surfactant $C_{12}E_5$, i.e. $CH_3(CH_2)_{11}(OCH_2CH_2)_5OH$ (Nikko Chemicals, Tokyo, Japan). Sample composition is given by the volume fraction of water ϕ_w, octane ϕ_o and surfactant ϕ_s. The specific heat is measured with a differential scanning microcalorimeter, MicroDSC II (Setaram, Caluire, France). While filling about 0.5 cm^3 mixture into the cylindrically shaped measurement cell, small changes of composition due to evaporation of oil and water can not be prevented. Care is taken to keep the contact period towards air as short as possible, i.e., a few seconds. After filling and weighting, the cells are closed for the measurement. Since there is also some air enclosed in the cells, neither pressure nor the volume remain constant during a temperature scan. Volume changes, however, are small, only arising due to the thermal expansion of the components.

The microcalorimeter measures the specific heat of the mixture relative to a reference system which is chosen to contain appropriate amounts of water and oil, but no surfactant. Hence, no absolute value for the specific heat is determined. Instead one obtains precise data for the relative specific heat per unit volume

$$C^{\mathrm{rel}}(T) \equiv \frac{\Delta Q}{\Delta T} \tag{1}$$

where ΔQ is the difference between the heat per unit volume absorbed by the sample and the reference system per temperature increment ΔT. Except for smoothening of data by averaging over several subsequent data points, which is automatically done by the microcalorimeter, no additional data treatment is applied. Typical heating rates are chosen in the range v_s=7...30 K h^{-1}. Since we are dealing with liquid (i.e., incompressible) samples which show no significant change of volume while passing phase boundaries, we interpret $C^{\mathrm{rel}}(T)$ as a variation of the specific heat at fixed volume, using the notation $C_v^{\mathrm{rel}}(T)$.

Overview of thermal curves

Figure 2a shows an optically determined phase diagram for equal volume fractions of water and oil, ϕ_w=ϕ_o, as function of temperature and surfactant concentration. For clarity we only give the surfactant range ϕ_s=0.05...0.25 contain-

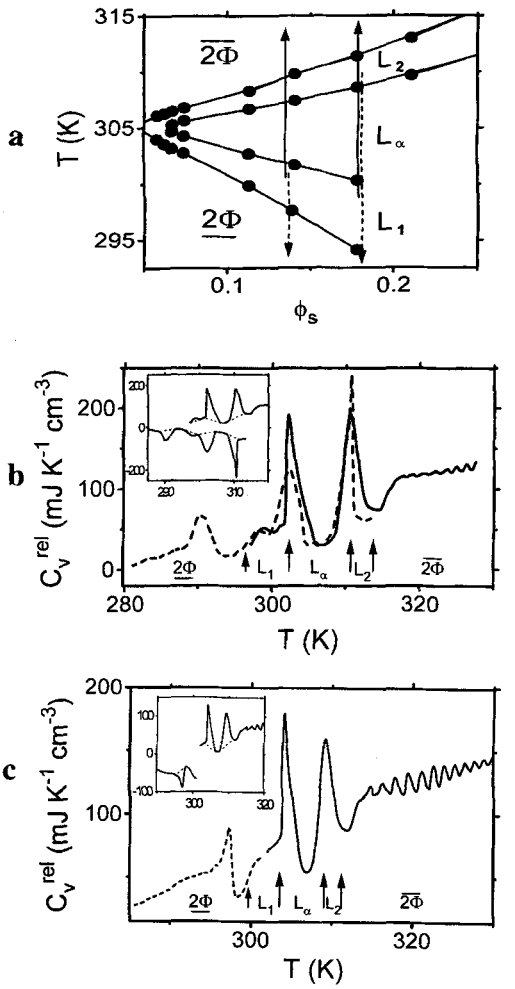

Fig. 2 Phase diagram and thermal curves for the system water, octane and $C_{12}E_5$. (a) Optically determined phase diagram for $\phi_w=\phi_o$. The solid and dashed lines indicate the paths of the measurements leading to the curves shown in parts (b) and (c). (b) Overview of complete up- (solid line) and down-scan (dashed line) of the temperature dependence of the difference in specific heat of a sample with composition $\phi_s=0.18$, $\phi_w=\phi_o=0.41$ relative to a reference system containing an appropriate amount of water and oil. At the bottom the structure of the mixture at different temperatures is indicated. The arrows indicate the optically determined phase boundaries. They differ slightly from those given in Fig. 2a, because different surfactant charges have been used for determining the optical phase diagram [14] and the calorimetric measurements. The inset indicates the choice of the baseline used to calculate the latent heat of the different transitions. Here, $-C_v^{rel}(T)$ is plotted for the down scan measurements, in order to avoid overlap of the curves. (c) The same data as in part (b) are given for the composition . $\phi_s=0.14$, $\phi_w=\phi_o=0.43$

ing the lamellar phase and the upper and lower microemulsion channels. In this temperature range the samples form liquid mixtures showing at least four phase transitions ($2\underline{\Phi}\rightarrow L_1\rightarrow L_\alpha\rightarrow L_2\rightarrow\overline{2\Phi}$) in a narrow temperature range around T. These transitions will be our primary interest in the following. The transitions between L_1 or L_2 and the respective lower and upper 2Φ-regions are determined by looking for changes in the turbidity of the mixtures forming a first sign of phase separation. The L_α-region corresponds to the temperature range where the mixture is birefrigent. It includes the coexistence regions of a lamellar with an L_1 and L_2-structure – in general the single phase L_α region is a much narrower region completely inside the one indicated in the figure. In contrast to the single phase L_α-structure, where birefringence is generally believed to indicate a lamellar structure, it is not obvious from visual inspection which structures are formed in the L_1- and L_2-regions. To clarify this point, small angle neutron scattering was performed on samples with $\phi_o=\phi_w$ and $\phi_s=0.189$ [33]. The data indicate that droplets are formed in both the L_1- and L_2-regions. They are in an disordered arrangement in the L_2- and in the upper part of the L_1-channel, while local order is observed close to the $2\underline{\Phi}$-L_1-boundary. For compositions close to this latter boundary also light scattering, small angle neutron scattering, viscosity and nuclear magnetic resonance measurements have been done by Olsson *et al.* [34–37], which support that droplets are formed. In addition, our experiments on the dynamics of the demixing at the L_2–$\overline{2\Phi}$ phase boundary [38] strongly suggest that the oscillations found in the curves when passing this boundary (cf. Fig. 2b, c) are only encountered when the structure close the upper emulsification boundary conforms to droplets. Hence, taking into account the symmetry of the phase behavior the present experimental evidence strongly suggests that droplet structures are found close to both, the *lower* ($2\underline{\Phi}$-L_1) and the *upper* (L_2-$\overline{2\Phi}$) *emulsification boundary*. It can not be excluded that for $\phi_s=0.14$ there is an additional change of morphology in the L_1- or L_2-channel so that the structure close to the L_α-region corresponds to e.g. a cylindrical or bicontinuous one. We will come back to this point below.

In accordance with the analogous sequence of phase changes, the thermal curves showing the temperature dependence of $C_v^{rel}(T)$ at different compositions are very similar. In the present paper we discuss curves of heating and cooling scans performed at $\phi_s=0.18$ and $\phi_s=0.135$. The path of the respective up scans are indicated by solid arrows in the phase diagram Fig. 2a, those of down scans by dashed ones. To be able to distinguish the solid and dashed lines, where the scans overlap, the arrows are slightly displaced to the left and right. We stress, however, that both measurements are performed on the same sample, i.e., they correspond to exactly the same composition of the mixture.

Figure 2b shows the thermal curves for the sample composition $\phi_w=\phi_o=0.41$ and $\phi_s=0.18$. The solid line indicates the variation of $C_v^{rel}(T)$ due to heating, while the dashed line shows the variation of $C_v^{rel}(T)$ due to cooling. For convenience the optically determined phase transition temperatures are marked by arrows below the thermograms. The curves show pronounced peaks in the vicinity

of phase transition temperatures in the single phase channel. We interpret the area under the peak as the heat absorbed during a phase transition, i.e., for first order phase transitions it corresponds to the latent heat of the transition. As required by thermodynamics all transitions are endothermic for up scans and exothermic for down scans; the difference in sign is due to the difference in sign of ΔT for the respective measurements. By its definition the relative specific heat does not change sign. Next we discuss the structure of the curves in more detail, identifying the phase transitions related to the different peaks.

For the heating scan the mixture is prepared and homogenized within the L_1-phase. Immediately after starting the scan at 296 K, i.e., still before the L_1 to L_α phase boundary, the signal for the specific heat goes through a small peak which is about 2.5 K wide. This peak will be attributed to the disappearance of local ordering of droplets in the L_1-region. The transition is therefore reminiscent to the melting of a glassy state in a colloidal system. The peak is followed by a significantly larger one extending from 301.5 to 306 K which we ascribe to the transition from the L_1 into the lamellar phase. It lies exactly on the optically determined transition temperature. In the subsequent subsections the form of the peak and its width will be described in more detail, arguing that its width corresponds to the width of the two-phase region accompanying the transition, while the area under the peak is related to the latent heat of the transition. The sample shows an suprisingly narrow single phase lamellar region of only 2.5 K width which is followed in the scan by another large peak (308.5–313.0 K) with a form which is nearly a mirror image of the former one. By comparison with the optically determined phase boundaries it is related to the change from the L_α into the L_2-phase. Within the L_2-phase no peak is visible until at about 314.5 K the emulsification boundary has been passed, so that one is in the $\overline{2\Phi}$-region. When passing this phase boundary with constant heating the signal for the specific heat increases, and subsequently it starts to oscillate. There is overheating for about 1.0 K leading to the observed difference in the optically determined boundary and the start of the increase. The osciallations are due to periodic instabilities of droplets, leading to formation of a coexisting water-rich phase. The dependence on composition and heating rate of the period and the heat absorbed during each oscillation is beyond the scope of the present paper. It has been discussed in Ref. [38].

The cooling scan (dashed line) starts within the L_2-phase. Again, both the L_2- to L_α- and the L_α- to L_1-phase boundary give rise to a peak in the specific heat. Due to hysteresis they are shifted towards slightly lower temperatures. These peaks are followed up by a small heat change within the L_1-phase, and a single peak in $C_v^{rel}(T)$ when passing the L_1 to $\underline{2\Phi}$, i.e, the lower emulsification boundary. There is significant overheating of about 3 K for this latter transition. For temperatures below the lower emulsification boundary oil droplets expel part of their interior phase, leading to a coexisting oil-rich phase. Contrary to the comparatively fast dynamics of formation of a water-rich phase the formation of an oil-rich one takes hours up to days.

The form of the curve in Fig. 2b is typical for a range of surfactant concentration around the chosen one. For comparison, in Fig. 2c the thermal curves of a mixture of composition ϕ_s=0.14 and ϕ_w=ϕ_o=0.43 are given. Again the solid line presents the variation of $C_v^{rel}(T)$ for a heating scan, while the dashed line gives the variation of $C_v^{rel}(T)$ for a cooling scan. The curve resembles the previous one. Again the transition from L_1 to the lamellar phase, and from there into the L_2-phase leads to large peaks in $C_v^{rel}(T)$. The temperature interval between these peaks, i.e., the width of the single phase lamellar region, decreases towards less than one degree, whereas the width of both two-phase regions is about 3 K.

Form and position of the larger peaks

In Fig. 3 the reproducibility of $C_v^{rel}(T)$ is shown for two successive up and down scans. For transparence $C_v^{rel}(T)$ is plotted positive for an up scan and negative for a down scan. The first up as well as down scan is given by a solid line and the second one by a dashed line. The first scan is started within the L_1-phase (296 K) and heated until 313.5 K. After equilibration for 10 min without stirring, the mixture is cooled down to 296 K. The second heating scan is started after equilibrating the mixture without stirring at 296 K for 30 min. As already stated, the corresponding curve is given by the dashed line. It is nearly indistinguishable from the first up scan. To investigate the influence of the equilibration period, the mixture is tempered for 2 h at 313.5 K before starting the second down scan. The result of the second cooling scan is shown by the dashed line in the lower part. The longer equilibration period influences slightly the shape of the first peak of the cooling scan ($L_2 \rightarrow L_\alpha$), which becomes somewhat sharper and steeper.

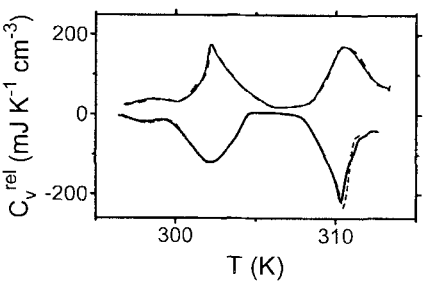

Fig. 3 Two successive up and down scans are shown to discuss the reproducibility of the measurements. To distinguish up and down scans, $C_v^{rel}(T)$ is plotted for the up scans while $-C_v^{rel}(T)$ is given for the down scans. The repective first scan is given by a solid, the second by a dashed line

For scan speeds from the experimentally accessible minimum scan speed of 7 K h^{-1} up to about 30 K h^{-1} the width and the height of the peaks do not change significantly. The curves reproduce very well when repeating the measurements, as long as one has not heated into the $\overline{2\Phi}$- or cooled into the $\underline{2\Phi}$-regions. Thus, the

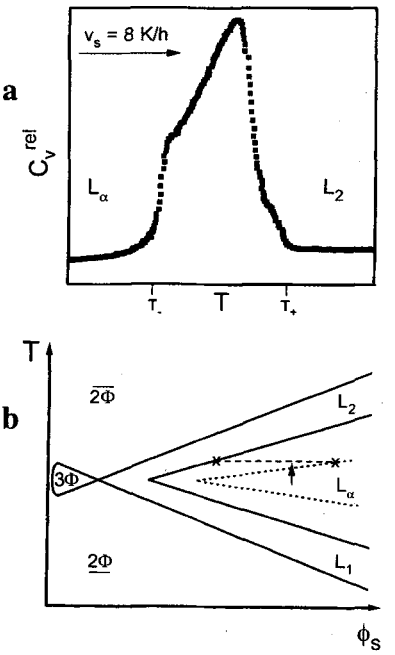

Fig. 4 Form of a peak in the specific heat related to an L_α to L_2 transition measured for a sample which has been equilibrated carefully in the lamellar phase (a). Sketch of the phase diagram with notations used to describe the temperature dependence of the coexisting mixtures in the two phase region associated with the transition (b)

transition within the L_1-channel and into the lamellar phase appear to be reversible and the finite width of the accompanying peaks is not due to the scan speed.

In contrast to the dependence on scan speed, the form of the peak depends on the history of the sample. In particular, we attribute the roundness of the second peak in a scan to the fact that the mixture has not completely relaxed to equilibrium in the very narrow lamellar region so that a significant number of defects remain in the structure which influence the following phase transition. At present we can not deal with these dynamical effects. Therefore, we will only discuss the form of a peak of a transition from a lamellar to a microemulsion phase (Fig. 4a) where the sample has been well equilibrated in the lamellar phase before starting the scan. First we note that there is a temperature interval of coexistence associated with a first order phase transition. For the experiment under consideration the lower and upper temperature of this coexistence region will be denoted by T_- and T_+, respectively. They might be slightly displaced with respect to the actual thermodynamic ones due to overheating. It will be assumed, however, that this effect is small so that the mixture is always close to equilibrium and the width of the two phase region $\Delta T \equiv T_+ - T_-$ does not differ significantly from the actual thermodynamic value. After passing T_- the mixture separates into two

phases of different structure and composition. For the purpose of getting a rough understanding about the physical mechanisms contributing to the peak we assume that $\phi_w=\phi_o$ still holds to a good approximation separately for both coexisting phases and make use of the phase diagram sketched in Fig. 4b. It is similar to Fig. 1, except that in this diagram the boundary of the single phase lamellar region is indicated by a dashed line. The path of the measurement is given by an arrow. The two coexisting compositions at a given temperature are marked by crosses at the borders of the respective single phase regions. The fractions formed by intersection of the arrow with the line connecting the crosses is directly related to the height of the meniscus in the sample. Note, that both the height of the meniscus as well as the composition of the coexisting phases change when changing temperature. These changes require work to be done to the sample which is reflected in the peak in $C_v^{rel}(T)$. This contribution to the specific heat is non-vanishing in the whole temperature range $[T_-,T_+]$, leading to a peak with a finite width and finite height. It is formed by a smooth positive function and bounded by steps to the baseline at T_- and T_+, respectively. The area under the peak corresponds to the heat absorbed in order to transform the lamellar into a microemulsion phase, i.e., it corresponds to the latent heat of the transition.

Heat changes

The area under a peak allows to estimate the heat change ΔQ related to a structural transition

$$\Delta Q = \int_{T_-}^{T_+} dT\,[C_v^{rel}(T) - C_{base}(T)] \tag{2}$$

where T_- corresponds to the beginning, and T_+ to the end of a peak. The choice for the baseline is shown by the dashed lines in the insets of Fig. 2b, c. An appropriate choice of the baseline is particularly difficult due to the narrowness of the single phase regions, due to the small peak within the L_1-region, and due to different values for a plateau of $C_v^{rel}(T)$ for different phases. For the present choice of $C_{base}(T)$ it is assumed that in analogy to the L_α to L_2 transition, the plateau value for a lamellar structure is well below that for an L_1-phase, and that $C_{base}(T)$ decreases linearly within the L_1-phase.

Table 1 Experimental values for the latent heat of transitions

ΔQ_{exp}/mJ cm^{-3}	L_1 to 2Φ	Small peak	L_1 to L_α	L_α to L_2
ϕ_s= 0.18, upscan		25±15	250±60	290±60
ϕ_s= 0.18, downscan	100±30	25±15	230±60	260±50
ϕ_s= 0.14, upscan			140±40	170±30
ϕ_s= 0.14, downscan	50±20			

In Table 1 the experimentally determined values for the heat absorbed when passing the lower emulsification boundary, the small peak within the L_1-phase, and either of the large ones, i.e. the transition from L_1 to L_α and from L_α to L_2, respectively, are listed. The values for the experimental errors mainly result out of uncertainties in how to determine the baseline $C_{base}(T)$. For ϕ_s=0.18 the values for the latent heat for the large peaks bounding the L_α-region are of the order of 0.25 J cm^{-3}, whereas the heat related to the small one within the L_1-phase is about one order of magnitude smaller. All values for the latent heat decrease under decreasing surfactant concentration.

Theory

In this section the experimentally determined values for the heat absorbed during a transition ΔQ_{exp} are compared to theoretical estimates ΔQ_{th}. The value for the latent heat of a first order phase transition can be calculated from the free energy, yielding

$$\Delta Q_{th} = \int_{T_-}^{T_+} \mathrm{d}T C_v(T)$$

$$= -\int_{T_-}^{T_+} \mathrm{d}T T \frac{\partial^2 F(T)}{\partial T^2}$$

$$= -\left(T_+ \frac{\partial F(T)}{\partial T}\bigg|_{T_+} - T_- \frac{\partial F(T)}{\partial T}\bigg|_{T_-} \right) + F(T_+) - F(T_-) \qquad (3)$$

where the last equation has been obtained by partial integration. Note that this expression for ΔQ_{th} only contains the values for the free energy and its first derivative with respect to temperature, evaluated at the borders T_- and T_+ of the coexistence region.

Since the transitions comprise changes of the structure and topology of the interface between water and oil, while the free energy of bulk water and oil hardly (if at all) changes during a transition, an effective free energy for the interface can be used to describe structural changes in the mixture [26, 29, 32, 39, 40]. In such a model it is assumed that the temperature and composition dependent properties of the oil-water interface determine the underlying microstructure. The surfactant molecules are assumed to build a two-dimensional incompressible extended monolayer separating water and oil domains. The most relevant contributions to the free energy result from the bending energy of the interface F_b, from the entropy of mixing of water and oil domains F_m in a microemulsion phase, and from the undulations of the monolayers F_u in a lamellar phase [26, 27, 29].

Interfacial free energy

The bending energy per unit volume characterizing the conformations of the surfactant monolayer is given by (cf. [32, 41])

$$\frac{1}{V}\int dA\left[\frac{\kappa}{2}\left(\frac{1}{R_1}+\frac{1}{R_2}-2c_0(T)\right)^2+\frac{\bar{\kappa}}{R_1R_2}\right] \tag{4}$$

where R_1^{-1} and R_2^{-1} are the principal curvatures which uniquely describe the local structure in the vicinity of any point A of the interface, while the bending modulus κ, the Gaussian modulus $\bar{\kappa}$ and the spontaneous curvature $c_0(T)$ are empirical material constants which will be discussed below. R_1 and R_2 denote the radii of two circles touching the interface at the point A (cf. Fig. 5). The respective tangents are chosen orthogonal, and the radii are such that in the vicinity of A the surface spanned by the two circles matches that of the interface up to second order. Specifying these radii for every point A uniquely describes the interface. A flat piece (Fig. 5a) corresponds to $R_1^{-1}=R_2^{-1}=0$; a piece curving towards oil or water (Fig. 5b) to a case where both radii are positive or negative, respectively; and a saddle structure (Fig. 5c) is characterized by radii of opposite sign.

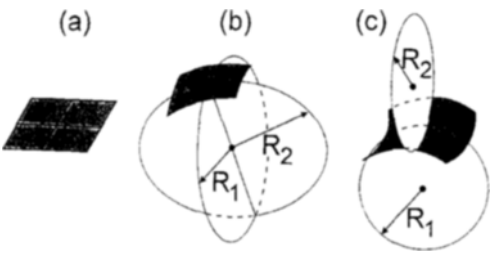

Fig. 5 Definition of the radii of curvature R_1 and R_2 describing the local structure of a piece of monolayer. In (a) a flat piece of monolayer is given, corresponding to $R_1^{-1}=R_2^{-1}=0$. (b) The situation where the monolayer bends towards one of the components, implying that R_1 and R_2 have the same sign which is chosen positive (negative) when the monolayer curves towards oil (water). (c) A saddle structure is characterized by radii of curvature with opposite signs

The bending moduli κ and $\bar{\kappa}$ describe the elastic energy needed to curve the interface away from its preferred average curvature specified by $c_0(T)$. They take values in the order of k_BT which hardly change with temperature. In accordance with [25, 32] we choose $\kappa\approx 0.8k_BT$ and $\bar{\kappa}\approx -0.4k_BT$, stressing, however, that these values are still under dispute [3, 4]. According to [14, 40] $c_0(T)$ depends to first order linearly on $\bar{T}-T$

$$c_0(T)=a(\bar{T}-T)\left(1+\frac{\bar{\kappa}}{2\kappa}\right)\equiv\alpha(\bar{T}-T) \tag{5}$$

where a=1.2 10^5 $K^{-1}cm^{-1}$ [14]. The second part of Eq. (5) introduces the shortcut α which allows to suppress the constant $(1+\bar{\kappa}/(2\kappa))$. Note that $c_o(T)$ has to be an odd function of $(T-\bar{T})$ due to the symmetry of the system under interchanging water and oil together with an appropriate change of temperature (cf. Fig. 1). The linear dependence of c_o on T is compatible with this symmetry; $\bar{T}$ corresponds to the symmetry line in the symmetric phase diagram and takes the value 305.6 K for the present system (Fig. 2a) [14]. Since $c_o(T)$ is an antisymmetric function in $T-\bar{T}$, the free energy is invariant under changing the temperature $T\rightarrow 2\bar{T}-T$ and exchanging simultaneously oil and water.

Table 2 Values for the mean H and Gaussian K curvature for flat lamellae, monodisperse spheres and cylinders. R_s and $R_c = 2/3\ R_s$ denote the radius of droplets and of cylinders, respectively. The volume fraction of the enclosed phase ϕ corresponds to $\phi_w+0.5\phi_s$ if water is enclosed and to $\phi_o+0.5\phi_s$ if oil is enclosed. For the investigated samples the volume fraction of water and oil are equal, leading to ϕ=0.5

	H	K
Water droplets in oil	$(R_s^w)^{-1} = -\frac{\phi_s}{3l_s\phi}$	$(R_s^w)^{-2}$
Water cylinders in oil	$\frac{1}{2}(R_c^w)^{-1} = -\frac{\phi_s}{4l_s\phi}$	0
Lamellar structure	0	0
Oil cylinders in water	$\frac{1}{2}(R_c^o)^{-1} = \frac{\phi_s}{4l_s\phi}$	0
Oil droplets in water	$(R_s^o)^{-1} = \frac{\phi_s}{3l_s\phi}$	$(R_s^o)^{-2}$

To find the free energy, Eq. (4) should be taken as a starting point to calculate the partition sum over all physically allowed conformations of the interface between water and oil. The resulting functional integral can not explicitly be solved, however. Therefore, we consider a mean field approximation involving the average mean curvature $H\equiv 0.5|A|^{-1}\int dA(R_1^{-1}+R_2^{-1})$ and the average Gaussian curvature $K\equiv|A|^{-1}\int dA R_1^{-1}R_2^{-1}$. The latter only depends on the topology of the surface due to the Gauss-Bonnet theorem [42]. Moreover, the total area $|A|$ of the interface can be expressed as $|A|/V=\phi_s/l_s$, by the volume fraction ϕ_s of surfactant, the length l_s=1.3 nm of the surfactant molecules [25, 43], and the volume V of the sample. With these relations and neglecting the contribution of fluctuations, the free energy per unit volume reduces to

$$F_b = \frac{2\kappa\phi_s}{l_s}(H - c_o)^2 + \frac{\phi_s}{l_s}\bar{\kappa}K \qquad (6)$$

For structures where the radii of curvature are the average the same for every point of the surface, i.e., for flat monolayers, monodisperse spheres and infinitely long monodisperse cylinders, the average curvatures H and K can easily be determined. Their values are listed in Table 2.

Fluctuations are believed to give important contributions to the free energy of lamellar structures, where the contribution due to undulations of the lamellae has been estimated [27, 44] to be

$$F_u = (k_B T)^2 \frac{\chi}{\kappa} \frac{\phi_s^3}{4 l_s^3} \left[\frac{1}{\phi_o^2} + \frac{1}{\phi_w^2} \right] \frac{1}{\phi_o + \phi_w} \tag{7a}$$

$$= (k_B T)^2 \frac{2\chi}{\kappa l_s^3} \frac{\phi_s^3}{(1-\phi_s)^3} \qquad \text{for } \phi_w = \phi_o = \frac{1-\phi_s}{2} \tag{7b}$$

The prefactor χ is still under debate [27, 35]. In agreement with [27] we choose χ=0.05, which is probably correct within a factor of 2 [35].

Besides fluctuations of the monolayer there are additional contributions to the free energy due to equivalent possibilities to realize surfaces with a given structure in space, e.g. there are many different possibilities to distribute a given set of droplets in space, giving rise to a free energy of mixing [27]

$$F_m = k_B T \frac{\phi_s^3}{6^3 l_s^3 \phi^3 (1-\phi)^3} [\phi \log\phi + (1-\phi) \log(1-\phi)] \tag{8a}$$

$$= -k_B T \frac{8 \log 2}{3^3 l_s^3} \phi_s^3 \qquad \text{for } \phi_w = \phi_o \tag{8b}$$

where ϕ corresponds to the volume fraction of enclosed phase, corresponding to ϕ_w+0.5ϕ_s if water is enclosed and to ϕ_o+0.5ϕ_s if oil is enclosed. For the investigated samples the volume fractions of water and oil are equal, leading to ϕ=0.5 which was used to arrive at part (b) of Eq. (8). Depending on concentration and microstructure, Eq. (8) may change slightly, due to a different dependence on composition. This does not affect our results, as in the following we are mainly interested in its temperature dependence. In all cases this free energy is only temperature dependent due to the factor $k_B T$ in front of the part describing the composition dependence.

Calculating the latent heat

The temperature dependence of the free energies per unit volume Eqs (6), (7) and (8) are shown in Fig. 6 for ϕ_s=0.14 and ϕ=0.5. The bending free energies for a droplet (F_s), cylindrical (F_c) and lamellar phase (F_l), respectively, are represented by solid lines (droplet phases), dotted lines (cylindrical phases) and a

dashed line (lamellar phase) [45]. For $\kappa<-2\bar{\kappa}$ the bending free energy of a cylindrical phase is always larger than those for a droplet or for a lamellar phase, implying that according to this theory a cylindrical structure is only formed for surfactants where $\kappa\geq-2\bar{\kappa}$. It has been shown in [32] that solely considering the bending free energy (6) permits to quantitatively calculate significant parts of the phase diagram. Besides the bending free energies for different structures, the contributions to the free energy due to entropy of mixing F_m and undulations of the lamellae F_u are shown in Fig. 6. The values of all free energies are close to each other. However, only the values for the bending free energies are strongly temperature dependent, whereas $F_u(T)$ and $F_m(T)$ are nearly constant within the investigated temperature interval. For this reason the contributions to the interfacial free energy per unit volume due to undulations of the lamellae Eq. (7) and due to mixing of water and oil domains Eq. (8) are negligible, for the description of the specific heat of the mixtures as it has already been suggested in previous work [25, 32].

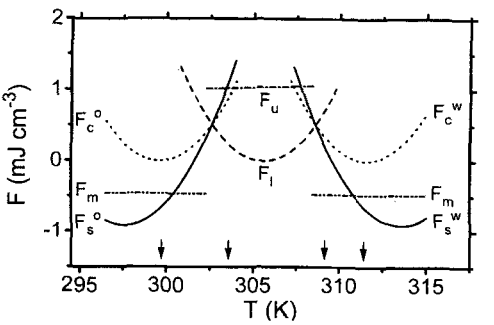

Fig. 6 Survey of different contributions to the free energies describing single phase mixtures with different morphologies. The different lines are described in detail in the text

In order to calculate the contribution of the bending free energy to the latent heat of a transition, we recall that the specific heat shows at worst a step at the boundaries of a peak (Fig. 4a). Since the specific heat is proportional to the second derivative $\partial^2 F/\partial T^2$, the corresponding free energy F is differentiable, and its values $F(T_+)$ and $F(T_-)$, as well as the corresponding derivatives $\partial/\partial T\, F(T)|_{T_+}$ and $\partial/\partial T\, F(T)|_{T_-}$ at the borders of the peak T_+ and T_- coincide with those determined from the free energies

$$F_-(T) = \frac{2\kappa\phi_s}{l_s}\left[H_- - c_o(T)\right]^2 + \frac{\phi_s}{l_s}\bar{\kappa}K_- \tag{9a}$$

$$F_+(T) = \frac{2\kappa\phi_s}{l_s}\left[H_+ - c_o(T)\right]^2 + \frac{\phi_s}{l_s}\bar{\kappa}K_+ \tag{9b}$$

of the single phase structures below and above the transition, respectively. Inserting these equations into Eq. (3) yields

$$\Delta Q_{\mathrm{th}} = 2\kappa \frac{\phi_s}{l_s}\left[-\alpha^2 (T_+^2 - T_-^2) + H_+^2 - H_-^2 - 2\alpha\bar{T}(H_+ - H_-) + \frac{\bar{\kappa}}{2\kappa}(K_+ - K_-)\right] \quad (10)$$

This expression can be put in a more convenient form by using that the free energies F_- and F_+ intersect at T_c, leading to

$$0 = F_+(T_c) - F_-(T_c) =$$

$$= 2\kappa\frac{\phi_s}{l_s}\left[2\alpha T_c(H_+ - H_-) + H_+^2 - H_-^2 - 2\alpha\bar{T}(H_+ - H_-) + \frac{\bar{\kappa}}{2\kappa}(K_+ - K_-)\right] \quad (11)$$

Note that the right hand side of Eqs (10) and (11) are equal except for the respective first term in square brackets. Inserting Eq. (11) into Eq. (10) leads to our final result

$$\Delta Q_{\mathrm{th}} = 4\kappa \frac{\phi_s}{l_s}\alpha T_c\left[(H_- - H_+) - \frac{T_+ + T_-}{2T_c}\alpha\Delta T\right] \quad (12)$$

where $\Delta T = T_+ - T_-$. There are two terms contributing to the heat which both have a simple interpretation:

$$\Delta Q_1 = \frac{4\kappa\alpha\phi_s}{l_s} T_c(H_- - H_+) \quad (13a)$$

$$\Delta Q_2 = \frac{4\kappa\alpha\phi_s}{l_s} T_c \frac{T_+ + T_-}{2T_c}\alpha\Delta T \approx \frac{4\kappa\alpha^2\phi_s}{l_s} T_c\Delta T \quad (13b)$$

The term ΔQ_1 corresponds to the heat $T_c\Delta S(T_c)$ where $\Delta S(T_c) \equiv (-\partial/\partial T)F_+(T)|_{T_c} + (\partial/\partial T)F_-(T)|_{T_c}$ is the difference of the slopes of the free energies F_+ and F_- at their intersection point T_c. This accounts for all of the latent heat when the width of the two phase region ΔT is negligible. Otherwise, there is a correction ΔQ_2, proportional to ΔT, which accounts for the fact that according to Eq. (3) the derivatives have to be taken at T_+ and T_-, respectively, instead of both at T_c. The second term of Eq. (3), involving the difference of the free energies at T_+ and T_- does not make an obvious contribution. In fact, one easily checks from the values given in Table 3 that the contributions of F_+ and F_- are much smaller than those arising from the derivatives. This, together with the fact that also the temperature derivatives of the undulation free energy F_u and the mixing free energy F_m are much smaller than those of the bending free energies, is the reason that the former free energies do not directly contribute to the latent heat of the phase transitions. Note however, that they influence the transition temperature T_c and the width of the coexistence region ΔT. Since the prefactors in F_u and F_m are

not known, these terms can not be discussed in detail. Neglecting the influence of F_u and F_m on T_c, however, only amounts to an error of about only 1%, and for the width of the transitions we have taken the experimental values determined from the temperature variation of the specific heat (cf. Fig. 2).

Comparison with experimental results

Before comparing the experimental values for the latent heat of the transitions with the theoretical predictions summarized in Table 3, we stress that the bending free energy can only account for transitions involving changes of the morphology of the surfactant layer. In particular, the loss of local ordering which we observed in the L_1-channel at ϕ=0.18 is probably not of this type. Moreover, the values given for the parameters l_s, κ, $\bar{\kappa}$ and $c_o(T)$ as well as for the prefactors in F_u and F_m are not yet accurate, although they are very likely close to the desired ones, because the temperature and composition dependent positions of phase boundaries are very well described [32]. The predictions for the transitions from a lamellar to an L_2 droplet phase (Table 3, last column of part IV) agree with

Table 3 Mean field predictions for the latent heat of transitions for $\phi = 0.5$. The values for the experimentally determined width of the two-phase regions ΔT are given, together with calculated values for ΔQ_1, ΔQ_2 and ΔQ_{th}. The errors given for ΔQ_2 and ΔQ_{th} only reflect the error in ΔT. The actual error will be larger, because the material constants l_s, κ, $\bar{\kappa}$ and α which were taken from the literature are also not yet precisely known. Since the accuracy of these parameters is not stated in the literature these errors could not be included

	ΔT/K	ΔQ_1/mJ cm^{-3}	ΔQ_2/mJ cm^{-3}	ΔQ_{th}/mJ cm^{-3}
I.		L_s^o to L_c^o		
ϕ_s = 0.18, upscan	2.6±0.5	120	120±25	0±25
ϕ_s = 0.18, downscan	3.0±0.5	120	140±25	−20±25
II.		L_s^o to L_α		
ϕ_s = 0.18, upscan	4.6±0.6	470	210±30	260±30
ϕ_s = 0.18, downscan	5.1±0.6	470	230±30	240±30
ϕ_s = 0.14, upscan	2.7±0.5	285	95±20	190±20
III.		L_c^o to L_α		
ϕ_s = 0.18, upscan	4.6±0.6	350	210±30	140±30
ϕ_s = 0.18, downscan	5.1±0.6	350	230±30	120±30
ϕ_s = 0.14, upscan	2.7±0.5	215	95±20	120±20
IV.		L_α to L_s^w		
ϕ_s = 0.18, upscan	4.7±0.5	480	220±25	260±25
ϕ_s = 0.18, downscan	3.8±0.4	480	180±20	300±25
ϕ_s = 0.14, upscan	3.5±0.5	290	125±20	165±20

the experimental values (Table 1, last column) and for ϕ_s=0.18 the experimental values for the droplet to lamellar transition are also well described. The situation is less clear for ϕ_s=0.14, where the experimentally determined value ΔQ_{exp}=140±40 mJ cm^{-3} agrees with the prediction ΔQ_{th}=120±20 mJ cm^{-3} for a transition from cylinders to a lamellar structure. This requires, that there is a transition from a droplet into a cylindrical structure in the temperature range T≈299...303 K which had been lost in the experiment due to too little overlap of the up- and down-scan measurements of the specific heat (cf. Fig. 2c).

Conclusion

We have given a survey over recent experimental and theoretical developments of the thermal characterization of phase transitions in water-oil-surfactant mixtures. As model surfactant we chose the nonionic surfactant $C_{12}E_5$. In contact with water and octane, it shows a nearly symmetric phase behavior, i.e., the properties of the mixtures hardly change under exchanging water and oil together with their respective volume fractions ϕ_w and ϕ_o, and simultaneously changing the temperature from T towards $2\bar{T}-T$. In a temperature interval of less than 20°C around $\bar{T}$ five structural transitions were observed in microcalorimetric measurements. With a high sensitivity the method detects phase transitions as well as the width of the corresponding two-phase regions. Moreover, for the first time it allows to measure the latent heat of a transition. Comparing the experimental data with the predictions of various models allows us to identify relevant contributions to a free energy describing the mixtures. In Ref. [25] it had been shown that for samples containing much more oil than water there is good agreement between experimental and theoretical results, allowing to fix the Gaussian bending modulus $\bar{\kappa}$ of the surfactant layer. For equal volume fractions of water and oil the data are less satisfactory. Due to the narrowness of the single phase regions and different plateau values of $C_v^{rel}(T)$ for different phases, an accurate measurement of the latent heat becomes increasingly difficult. In order to improve these data the understanding of the step in $C_v^{rel}(T)$ has to be enhanced in order to identify the proper choice of the baseline needed to calculate the values for the latent heats. For a quantitative comparison with theoretical predictions corrections involving the width of the transitions have been derived. In the present work the width has been taken from experiment. Here, further refinement of the models is needed to also work out the predictions for the width of the transitions. Still, even in the present early stage of the calorimetric investigation of microemulsions there is quantitative agreement between experimental results and theoretical predictions. The direct relation between calorimetric data and a theoretical modeling of the phase behavior will have a significant impact on the further developments of the understanding of microemulsions.

* * *

The authors are indebted to T. Sottmann for help with the measurements, and to M. Maskos for carefully reading the manuscript. They thank M. Schmidt and B. Widom for stimulating discussions. D. V. and the J. V. acknowledge financial support of the Deutsche Forschungsgemeinschaft.

References

1 W. M. Gelbart, A. Ben-Shaul and D. Roux, Micelles, Membranes, Microemulsions, and Monolayers, Springer, New York 1994.
2 M. Kahlweit, R. Strey and G. Busse, J. Phys. Chem., 94 (1990) 3881.
3 T. Sottmann and R. Strey, J. Phys. Condens. Matter, 8 (1996) A39.
4 F. Sicoli, D. Langevin and L. T. Lee, J. Chem. Phys., 99 (1993) 4759.
5 P. D. I. Fletcher and D. I. Horsup, J. Chem. Soc. Faraday Trans., 88 (1992) 855.
6 P. G. de Gennes and C. Taupin, J. Phys. Chem., 86 (1982) 2294.
7 G. Gompper and M. Schick, in: C. Domb and J. L. Lebowitz edts, Phase Transitions and Critical Phenomena, Vol. 16, Academic Press, London 1994.
8 H. J. Davies, J. F. Bodet, L. E. Scriven and W. G. Miller, in: J. Meunier et al. edts, Physics of amphiphilic layers, Springer Proc. Phys., 21 (1987).
9 R. Strey, Ber. Bunsenges. Phys. Chem., 97 (1993) 742.
10 M. Kahlweit and R. Strey, Angew. Chem. Int. Ed., 24 (1985) 654.
11 S.-H. Chen, S.-L. Chang and R. Strey, J. Chem. Phys., 93 (1990) 1907.
12 W. K. Kegel and H. N. W. Lekkerkerker, J. Phys. Chem., 97 (1993) 11124.
13 M. Borkovec, H.-F. Eicke, H. Hammerich and B. Das Gupta, J. Phys. Chem., 92 (1988) 206.
14 R. Strey, Coll. Polym. Sci., 272 (1994) 1005.
15 M. Kotlarchyk, S.-H. Chen, J. S. Huang and M. W. Kim, Phys. Rev. A, 29 (1984) 2054.
16 P. Speiser in: P. L. Luisi and B. E. Straub edts, Reverse Micelles, Plenum Press, New York 1984, p. 339; B. H. Robinson, A. N. Khan-Lodhi and T. Tower, in: M. P. Pilini edt, Structure and Reactivity in Reverse Micelles, Elsevier, Amsterdam 1989; J. Traber, in D. O. Shah edt, Surface Phenomena in Enhanced Oil Recovery, Plenum Press, New York 1981.
17 W. Jahn and R. Strey, J. Phys. Chem., 92 (1988) 2294.
18 D. Bedeaux and G. J. M. Koper, Physica A, 194 (1993) 105.
19 E. W. Kaler, K. E. Bennett, H. T. Davis and L. E. Scriven, J. Chem. Phys., 79 (1983) 5673.
20 R. Strey, O. Glatter, K. V. Schubert and E. W. Kaler, J. Chem. Phys., 105 (1996) 1175.
21 S. Clark, P. D. I. Fletcher and X. Ye, Langmuir, 6 (1990) 1301.
22 P. Honorat, D. Roux and A. M. Bellocq, J. Physique Lett., 45 (1984) 961.
23 E. Z. Radlinska, S. T. Hyde and B. W. Ninham, Langmuir 5, (1989) 1427.
24 D. Vollmer and P. Ganz, J. Chem. Phys., 103 (1995) 4697.
25 D. Vollmer and R. Strey, Europhys. Lett., 32 (1995) 693.
26 S. A. Safran, L. A. Turkevich and P. Pincus, J. Physique, 45 (1984) L-69.
27 D. Andelman, M. E. Cates, D. Roux and S. A. Safran, J. Chem. Phys., 87 (1987) 7229.
28 L. Golubovic and T. C. Lubensky, Phys. Rev. A, 41 (1990) 4343.
29 J. Daicic, U. Olsson and H. Wennerström, Langmuir, 11 (1995) 2451.
30 H. Wennerström, J. Daicic, U. Olsson, G. Jerke and P. Schurtenberger, J. Mol. Liq., in press.
31 P. Pieruschka and U. Olsson, Langmuir, 12 (1996) 3362.
32 D. Vollmer, J. Vollmer and R. Strey, Phys. Rev. E, 54 (1996) 3028; erratum in press.
33 T. Sottmann and R. Strey, unpublished.
34 U. Olsson and P. Schurtenberger, Langmuir, 9 (1993) 3389.
35 H. Bagger-Jörgensen, U. Olsson and K. Mortensen, Langmuir, 12 (1996) 4057.
36 M. S. Leaver and U. Olsson, Langmuir, 10 (1994) 3449.

37 M. S. Leaver, U. Olsson, H. Wennerström and R. Strey, J. Phys. II, 4 (1994) 515.
38 D. Vollmer, J. Vollmer and R. Strey, Europhys. Lett., 39 (1997) 245; D. Vollner, R. Strey and J. Vollner, J. Chem. Phys., 107 (1997) 3619; J. Vollmer, D. Vollmer and R. Strey, J. Chem. Phys., 107 (1997) 3627. Note the different convention for the sign of the radii in these papers.
39 S. A. Safran, in: S. H. Chen et al. edts, Structure and Dynamics of Strongly Interacting Colloids and Supramolecular Aggregates in Solution, Kluwer, Amsterdam 1992.
40 U. Olsson and H. Wennerström, Adv. Coll. Interf. Sc., 49 (1994) 113.
41 P. B. Canham, J. Theor. Biol., 26 (1970) 61; W. Helfrich, Z. Naturf., C28 (1973) 693; E. Evans, Biophys. J., 14 (1974) 923.
42 C. Nash and S. Sen, Topology and Geometry for Physicists, Academic Press, London 1983.
43 Also different values for the length of the surfactant molecules have been given in the literature, cf. Ref. [20].
44 W. Helfrich, Z. Naturf., 33a (1978) 305.
45 For all structures the mean field approximation to the bending free energy yields parabolic functions of temperature (cf. Fig. 6). It might seem disturbing that the entropies calculated as the first temperature derivative from these free energies take negative values to the right of the minimum of the parabolae. Note however, that we are dealing with effective free energies which only take into account degrees of freedom of the geometry of the interface between water and oil. The corresponding entropy is only defined up to a constant. An arbitrary linear function in temperature may be added to the free energy. Doing this leads to positive values of the entropy in any physically relevant range of parameters without influencing the predictions on the phase boundaries and the latent heat of transitions.